Stem Cell Reports
Article

ISSCR

OPEN ACCESS

Alkaline Ceramidase 1 Protects Mice from Premature Hair Loss by Maintaining the Homeostasis of Hair Follicle Stem Cells

Chih-Li Lin,[1,2,3] Ruijuan Xu,[1,2] Jae Kyo Yi,[1,2,3] Fang Li,[1,2] Jiang Chen,[1,3] Evan C. Jones,[4] Jordan B. Slutsky,[4] Liqun Huang,[1] Basil Rigas,[1] Jian Cao,[1,3] Xiaoming Zhong,[5] Ashley J. Snider,[1,2,3] Lina M. Obeid,[1,2,3] Yusuf A. Hannun,[1,2,3] and Cungui Mao[1,2,3,4,*]

[1]Department of Medicine, Stony Brook University, Stony Brook, NY, USA
[2]Department of Medicine and Stony Brook Cancer Center, Stony Brook University, HSC T15-023, Stony Brook, NY 11794, USA
[3]Graduate Program in Molecular and Cellular Biology, Stony Brook University, Stony Brook, NY, USA
[4]Department of Dermatology, Stony Brook University, Stony Brook, NY, USA
[5]Industrial Technology Research Institute, Zhejiang University, Hangzhou, Zhejiang Province, China
*Correspondence: cungui.mao@stonybrook.edu
https://doi.org/10.1016/j.stemcr.2017.09.015

SUMMARY

Ceramides and their metabolites are important for the homeostasis of the epidermis, but much remains unknown about the roles of specific pathways of ceramide metabolism in skin biology. With a mouse model deficient in the alkaline ceramidase (*Acer1*) gene, we demonstrate that ACER1 plays a key role in the homeostasis of the epidermis and its appendages by controlling the metabolism of ceramides. Loss of *Acer1* elevated the levels of various ceramides and sphingoid bases in the skin and caused progressive hair loss in mice. Mechanistic studies revealed that loss of *Acer1* widened follicular infundibulum and caused progressive loss of hair follicle stem cells (HFSCs) due to reduced survival and stemness. These results suggest that ACER1 plays a key role in maintaining the homeostasis of HFSCs, and thereby the hair follicle structure and function, by regulating the metabolism of ceramides in the epidermis.

INTRODUCTION

The mammalian epidermis is the largest organ, consisting of the interfollicular epidermis (IFE) with the pilosebaceous unit attached, including the hair follicle (HF) and sebaceous gland (SG). The homeostasis of the different compartments of the epidermis is maintained by distinct adult stem cell populations residing in specialized niches (Hsu et al., 2014). Stem cells in the basal layer of the IFE generate transit-amplifying cells, which, upon ceasing proliferation, migrate toward the skin surface to differentiate sequentially into the spinous layer, granular layer, and cornified layer (also known as stratum corneum) (Fuchs, 2007). The epidermal permeability barrier (EPB) is established in the stratum corneum to protect the body of a mammal from outside-in threatening allergens or pathogens while preventing inside-out water or body fluid loss. Growing hair from the epidermis is another important and protective function of the skin (Sotiropoulou and Blanpain, 2012). Hair grows out from and is maintained in the HF, which cycles through three distinct stages: the growing stage (anagen), regression stage (catagen), and resting stage (telogen) (Alonso and Fuchs, 2006). Hair growth and reactivation of the HF cycle are executed by stem cells residing in the specific bulge region in HFs. Stem cell homeostasis should be tightly regulated for proper HF cycling and hair growth (Sotiropoulou and Blanpain, 2012), because mutations of genes involved in stem cell homeostasis can cause hair loss, namely alopecia (Nakamura et al., 2013).

Ceramides, a group of sphingolipids, play a key role in maintaining the structure and function of the epidermis (Pappas, 2009). In addition, ceramides and their metabolites sphingosine and sphingosine-1-phosphate (S1P) can act as bioactive lipids to mediate various biological processes (Hannun and Obeid, 2008; Mao and Obeid, 2008). Ceramides are synthesized by the action of ceramide synthases encoded by six distinct genes (*CERS1–6*) in mammals (Levy and Futerman, 2010). Different CERS isoforms use acyl-CoAs of different chain lengths as substrates, so ceramide species differing in acyl-chain length are synthesized in mammalian cells (Grösch et al., 2012). Jennemann et al. (2012) demonstrate that knocking out the ceramide synthase 3 responsible for the biosynthesis of ultra-long-chain ceramides impairs the EPB, resulting in the death of newborns. Knocking out ceramide synthase 4 responsible for the biosynthesis of long-chain (LC) ceramides reduces the hair follicle stem cell (HFSC) population and results in hair loss in mice without affecting the EPB (Ebel et al., 2014; Peters et al., 2015). These animal studies strongly suggest that different ceramides play important and distinct roles in maintaining the homeostasis of different compartments of the epidermis.

Once synthesized, ceramides can be hydrolyzed into sphingosine (SPH) by the action of ceramidases encoded by five distinct genes, the acid ceramidase (*ASAH1/Asah1*), neutral ceramidase (*ASAH2/Asah2*), alkaline ceramidase 1 (*ACER1/Acer1*), alkaline ceramidase 2 (*ACER2/Acer2*), and alkaline ceramidase 3 (*ACER3/Acer3*) (Mao and Obeid, 2008). ACER1 is a member of the alkaline

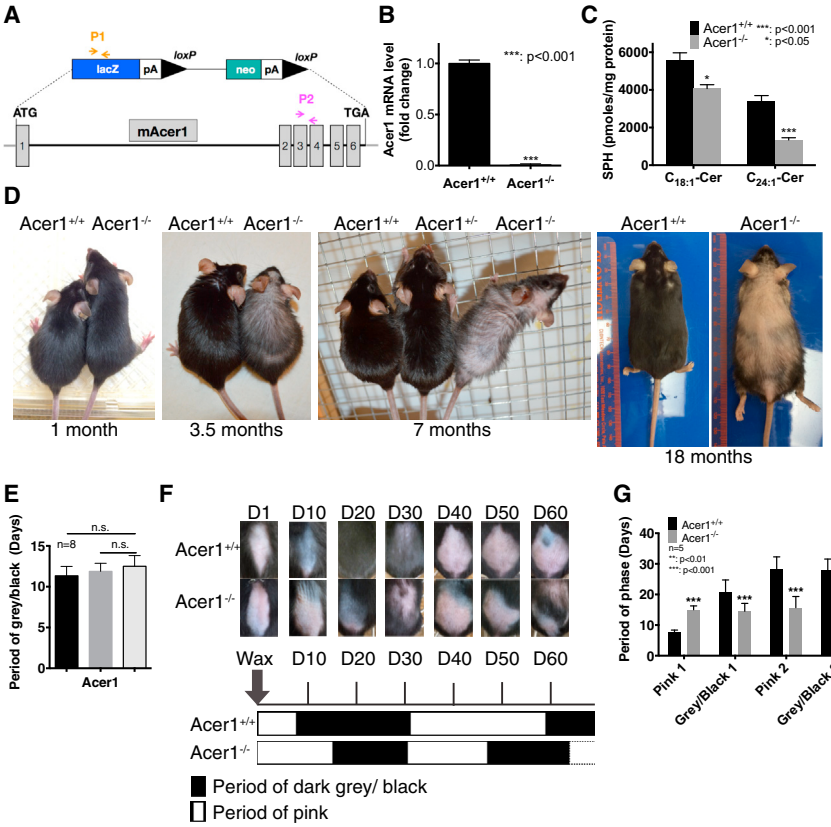

Figure 1. Knockout of *Acer1* in C57BL/6 Mice Induces Progressive Alopecia

(A) The *Acer1* gene targeting strategy. The *Acer1* ORF was replaced by the gene cassette containing the *LacZ* and *Neo* genes. ATG, the translation start codon; TGA, the translation stop codon; P1, the primer pair for the LacZ gene; P2, the PCR primer pair for Exon3/4 of the *Acer1* gene.

(B) *Acer1* mRNA levels in $Acer1^{+/+}$ and $Acer1^{-/-}$ mouse skin tissues. n = 3 individual mice.

(C) ACER1 enzymatic activity on $C_{24:1}$ ceramide or $C_{18:1}$ ceramide in $Acer1^{+/+}$ and $Acer1^{-/-}$ mouse skin tissues. n = 3 individual mice.

(D) Female mice of different ages and genotypes.

(E) The length (in days) of the first anagen (gray/black) of the hair growth cycle among $Acer1^{+/+}$, $Acer1^{+/-}$, and $Acer1^{-/-}$ mice. N.s., not significant.

(F) The images of dorsal skins taken from P122 $Acer1^{+/+}$ and $Acer1^{-/-}$ mice from day 1 (D1) to day 60 (D60) post depilation by waxing.

(G) The length of telogen (pink) and anagen (dark gray/black) following depilation on P122 mice.

The error bars indicate the SD.

ceramidase family that was identified by our group initially from the yeast *Saccharomyces cerevisiae* and then from mammals. *Acer1* is predominantly expressed in the skin (Houben et al., 2006; Mao et al., 2003; Sun et al., 2008). Our previous studies found that *Acer1* is highly expressed in differentiating (spinous layer) and differentiated epidermal keratinocytes (granular layer), but its expression is low in proliferative keratinocytes in the basal layer (Houben et al., 2006), indicating that ACER1 may have a role in epidermal differentiation. Indeed, with *in vitro* cell-culture systems, we demonstrate that ACER1 may mediate growth arrest and differentiation of human epidermal keratinocytes by regulating the hydrolysis of cellular ceramides (Sun et al., 2008). However, its physiological roles in regulating the metabolism of epidermal ceramides and the homeostasis of the epidermis remain unclear.

In this study, using mouse genetic approaches in combination with biochemical analyses, we demonstrate that ACER1, the mouse ortholog of human ACER1, is expressed in the IFE, SG, and HF and plays a key role in maintaining the homeostasis of these epidermal compartments. We reveal that *Acer1* deficiency increases the levels of ceramides and SPH in the skin and progressively depletes HFSCs, thereby resulting in progressive alopecia. These results suggest that ACER1 plays a key role in regulating the homeostasis of the epidermis by controlling the catabolism of ceramides in epidermal compartments.

RESULTS

Loss of *Acer1* Decreases Alkaline Ceramidase Activity in Epidermis and Leads to Progressive Alopecia

To study the role of ACER1 in regulating the homeostasis of the epidermis, we generated an *Acer1* knockout mouse line by replacing the entire coding region of the *Acer1* gene with the reporter/selection cassette containing the *LacZ* and *Neo* genes (Figure 1A). Interbreeding mice heterozygous for the *Acer1* null allele, $Acer1^{+/-}$ mice, gave rise to wild-type (WT) mice ($Acer1^{+/+}$), heterozygous $Acer1^{+/-}$, and mice homozygous for the *Acer1* null allele ($Acer1^{-/-}$) at the expected Mendelian ratio (+/+:+/−:−/−, 46:107:47), suggesting the absence of significant embryonic lethality. RT-qPCR showed that no coding sequence of the *Acer1* gene is transcribed in the skin tissues of $Acer1^{-/-}$ mice on postnatal day 4 (P4) (Figure 1B). Consistently, alkaline ceramidase activity on the very-long-acyl-chain (VLC) ceramide $C_{24:1}$ ceramide ($C_{24:1}$-Cer), a preferred substrate of ACER1 (Sun

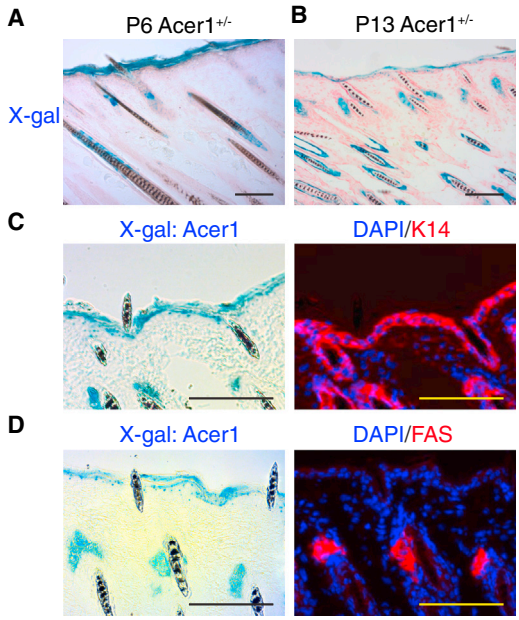

Figure 2. *Acer1* Is Expressed in Multiple Compartments of the Mouse Skin

(A and B) X-gal staining of cryosections of the skin of P6 (A) and P13 (B) *Acer1*$^{+/-}$ mice. The X-gal signals are shown in blue, and tissue sections were counterstained with eosin (A) or nuclear fast red (B).

(C and D) Two consecutive skin cryosections from a P13 *Acer1*$^{+/-}$ mouse were stained with X-gal (the left panel) or antibody specific for K14 (C) or FAS (D), and counterstained for nuclei with DAPI (blue).

Scale bar, 100 μm.

et al., 2008), was markedly decreased in the skin tissues of P4 *Acer1*$^{-/-}$ mice, compared with *Acer1*$^{+/+}$ littermates (Figure 1C). In contrast, *Acer1* knockout only moderately decreased skin alkaline ceramidase activity on the LC ceramide $C_{18:1}$ ceramide (Figure 1C). These results suggest that *Acer1* encodes major and minor skin alkaline ceramidase activity on VLC ceramide and LC ceramide, respectively.

To assess the role of ACER1 in skin homeostasis, we followed the gross morphological features of *Acer1*$^{+/+}$, *Acer1*$^{+/-}$, and *Acer1*$^{-/-}$ C57BL/6J mice up to 18 months of age. *Acer1*$^{-/-}$ mice showed no difference in body size (Figure 1D) and body weight (Figure S1A) from age- and sex-matched *Acer1*$^{+/+}$ or *Acer1*$^{+/-}$ littermates at young ages (1–7 months old; Figure S1A). However, at middle ages (13 and 18 months old; Figure S1A), *Acer1*$^{-/-}$ mice had lower body weight than *Acer1*$^{+/-}$ and *Acer1*$^{+/+}$ mice, which showed no difference in body weight. Necropsy showed that *Acer1*$^{-/-}$ mice were similar with regard to anatomy and size of major organs, including heart, brain, liver, lungs, kidneys, and spleens, compared with *Acer1*$^{+/+}$ or *Acer1*$^{+/-}$ mice (data not shown). Intercrossing of *Acer1*$^{-/-}$ mice gave rise to a similar litter number and size to the intercross of *Acer1*$^{+/+}$ mice (Figure S1B). These results suggest that *Acer1* knockout does not affect mouse development, fertility, and general health. However, in contrast to *Acer1*$^{+/+}$ and *Acer1*$^{+/-}$ mice, *Acer1*$^{-/-}$ mice developed progressive hair loss starting at 2–3 months of age (Figure 1D), suggesting that ACER1 is essential for the hair growth and/or maintenance.

Loss of *Acer1* Disturbs Hair Follicle Cycling

Since a disruption of HF cycling has been implicated in progressive hair loss (Courtois et al., 1994), we examined if *Acer1* deficiency affects HF cycling. By tracing the cyclic changes of the dorsal skin color in mice, we found that there was no difference in hair cycling among *Acer1*$^{+/+}$, *Acer1*$^{+/-}$, and *Acer1*$^{-/-}$ mice up to 2 months of age (Figure 1E). Since the hair loss phenotype becomes more discernible in *Acer1*$^{-/-}$ mice at 3–4 months of age or older (Figure 1D), we investigated if loss of *Acer1* affects HF cycling in mice at these ages. Although in rodents, synchronized HF growth occurs in waves that sweep dorsally, as the mouse ages, the waves occur less frequently and only in small patches (Stenn and Paus, 2001). This makes it difficult to evaluate the effect of *Acer1* deficiency on HF cycling in mice older than 2 months. To this end, we depilated hair from the dorsal skin in P122 mice using a waxing technique (Muller-Rover et al., 2001) to synchronize hair cycling. After waxing-induced synchronization, we found that the transition of the first telogen to anagen was significantly delayed in *Acer1*$^{-/-}$ mice compared with *Acer1*$^{+/+}$ mice (Figures 1F, 1G, and S2). However, after the first cycle, both telogen and anagen were much shorter in *Acer1*$^{-/-}$ mice compared with *Acer1*$^{+/+}$ mice (Figures 1F, 1G, and S2), suggesting that loss of *Acer1* accelerates HF cycling.

Acer1 Is Expressed in Multiple Skin Compartments

In *Acer1*$^{+/-}$ or *Acer1*$^{-/-}$ mice, the promoter-less lacZ reporter gene is placed downstream of the *Acer1* promoter, so the expression of the *LacZ* gene is under the control of the endogenous *Acer1* promoter. This allowed us to examine the expression of *Acer1* by following lacZ gene-encoded β-galactosidase activity, which can be detected by *in situ* X-gal staining. We found X-gal stain in the IFE, HF, and SG in both P6 (Figure 2A) and P13 *Acer1*$^{+/-}$ mice (Figure 2B). P56 *Acer1*$^{+/-}$ mice exhibited a similar X-gal staining pattern to P13 *Acer1*$^{+/-}$ mice (Figure S3A). These compartment-specific expression patterns were confirmed by immunofluorescent staining (IF) with antibodies against compartment-specific markers, including the IFE basal layer marker K14 and the SG marker fatty acid synthase (FAS) (Figures 2C and 2D). X-gal stain was absent in the bladder, brain, colon, heart, kidney, liver, lung, pancreas, small

intestine, spleen, stomach, seminal vesicle, and testis from P56 *Acer1*$^{+/-}$ mice (Figure S3A) and P56 *Acer1*$^{+/+}$ skin (Figure S3B). These results suggest that ACER1 is a skin-specific ceramidase that is highly expressed in all the major compartments of the epidermis.

Loss of *Acer1* Alters Skin Sphingolipids

To determine the role of ACER1 in regulating the metabolism of sphingolipids in the skin, we compared the levels of various types of sphingolipids in skin tissues in adult *Acer1*$^{+/+}$ and *Acer1*$^{-/-}$ mice. In P33 adult mouse skin, loss of *Acer1* increased the levels of ceramides carrying saturated LC or VLC ($C_{16:0}$, $C_{20:0}$, $C_{22:0}$, $C_{24:0}$, and $C_{26:0}$) and total ceramides but not ceramides carrying unsaturated VLCs ($C_{24:1}$ or $C_{26:1}$) (Figure 3A) or dihydroceramides (Figure 3B). Loss of *Acer1* also substantially increased the levels of various phytoceramides (Figure 3C) and α-hydroxyceramide species (Figure 3D) in the adult skin. Interestingly, loss of *Acer1* did not affect the levels of the complex sphingolipids, mono-hexosylceramides (Figure 3E) or sphingomyelins (Figure 3F) in the adult skin. Unexpectedly, loss of *Acer1* markedly increased the levels of sphingoid bases, including sphingosine (SPH), dihydrosphingosine (DHS), and phytosphingosine (PHS) (Figure 3G) without affecting their phosphates in the adult skin (Figure 3H).

To investigate whether the unexpected increases in sphingoid bases resulted from compensatory changes in the expression of other sphingolipid-metabolizing enzymes, we performed a qPCR array that simultaneously quantifies mRNA levels of major enzymes involved in the metabolism of sphingolipids. The results demonstrated that *Acer1* loss altered mRNA levels of multiple enzymes (Figure S4). With qPCR for analyzing individual genes, we confirmed that *Acer1* loss indeed increased the mRNA levels of *Acer2*, *Acer3* (Figure 3I), and S1P phosphatase 2 (*Sgpp2*) (Figure 3J) while decreasing the mRNA levels of acid ceramidase (Asah1), neutral ceramidase (*Asah2*) (Figure 3I), sphingosine kinase 1 (*Sphk1*), and sphingosine kinase 2 (*Sphk2*) (Figure 3K). These results may explain why *Acer1* loss increases rather than decreases its products. Taken together, these results suggest that ACER1 regulates the levels of various types of ceramides and sphingoid bases in the mouse skin.

Loss of *Acer1* Promotes Both Cell Proliferation and Apoptosis in the Epidermis

Increasing numbers of studies demonstrate that ceramides with different acyl chains might have distinct roles in mediating biological responses. VLC ceramides, such as C_{24} and $C_{24:1}$ ceramides, have been shown to promote cell proliferation and cell survival whereas LC ceramides, such as C_{16} and C_{18} ceramides, exert the opposite effects (Grösch et al., 2012). In addition, SPH has been shown to inhibit cell proliferation and to induce cell differentiation or apoptosis (Cuvillier, 2002; Hu et al., 2010; Xu et al., 2006, 2016). Since loss of *Acer1* altered the levels of various ceramides and SPH in mouse skin, we investigated whether loss of *Acer1* affected cell proliferation, differentiation, and apoptosis in different epidermal compartments. Immunohistochemistry (IHC) revealed that compared with P33 *Acer1*$^{+/+}$ mice, their *Acer1*$^{-/-}$ littermates had more cells stained positively for Ki-67, a proliferation marker, in the IFE basal layer, HF, and SG (Figures 4A and 4B). Consistently, western blot analyses showed that compared with *Acer1*$^{+/+}$ mice, *Acer1*$^{-/-}$ mice had increased expression of PCNA (another proliferation marker), cytokeratin 14 (K14; a marker of basal layer keratinocytes in the IFE, HF, and SG), and FAS (an SG marker) and decreased expression of K10 and involucrin, differentiation markers for the granular layer and spinous layer, respectively, in the epidermis (Figure S5A). qPCR analyses found that compared with their *Acer1*$^{+/+}$ littermates, P33 *Acer1*$^{-/-}$ mice had decreased mRNA levels of K10 and involucrin in the epidermis (Figure S5B). Terminal deoxynucleotidyl transferase dUTP nick end labeling (TUNEL) assays found more apoptotic cells in the *Acer1*$^{-/-}$ epidermis, especially in the HF infundibulum region (Figures 4C and 4D). Taken together, these results suggest that *Acer1* deficiency increases both cell proliferation and apoptosis while decreasing cell differentiation in the epidermis, suggesting a role in regulating the homeostasis of the major epidermal compartments.

ACER1 Alters the Morphology of the Hair Follicle Infundibulum and Sebaceous Gland but Not the Number of Hair Follicles

Acer1$^{-/-}$ mice exhibited a progressive alopecia phenotype (Figure 1D), suggesting a role for ACER1 in regulating hair growth or maintenance. As hair growth and maintenance depend on the homeostasis of the HF, we investigated whether *Acer1* deficiency reduced the number of HFs and/or altered their morphology. H&E staining showed that the pilary canal in the HF infundibulum region was wider and morphologically irregular in *Acer1*$^{-/-}$ mice compared with that in *Acer1*$^{+/+}$ mice (Figure 4E), although the HF numbers were similar in these mice (Figure S5C).

Because *Acer1* is highly expressed in the SG and an abnormality in the SGs could also lead to hair loss, we investigated if loss of *Acer1* affected the function or morphology of the SG. We performed oil red O (ORO) staining to monitor lipid secretion from SG. As shown in Figure S5D, loss of *Acer1* reduced ORO staining on the surface of the skin while enhancing ORO staining in the HF pilary canal, suggesting that *Acer1* deficiency may impair lipid secretion from the SG to the skin surface. The accumulation of lipids in the opening of the pilary canal may be responsible for the dilation of the HF infundibulum in *Acer1*$^{-/-}$ mice.

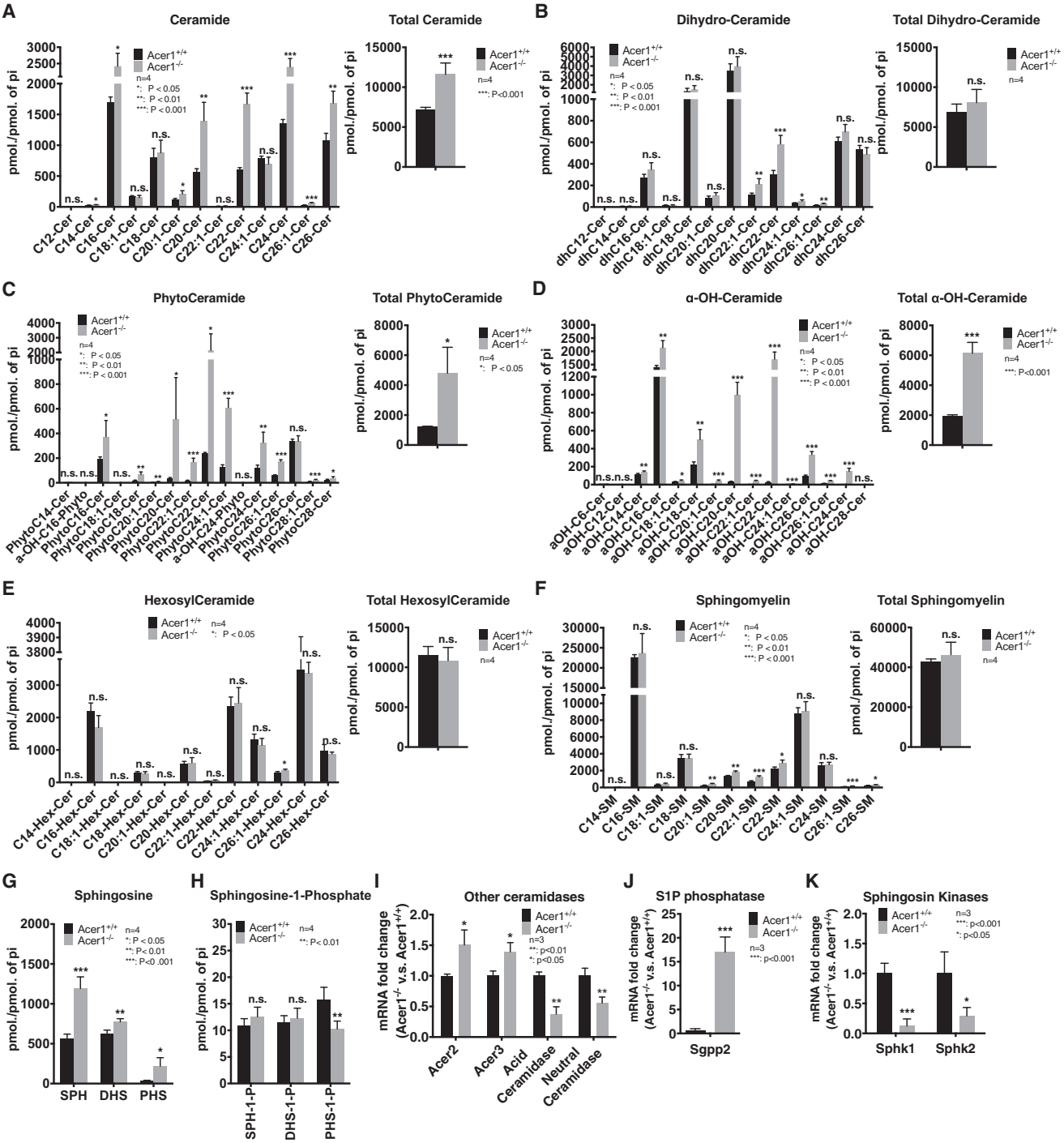

Figure 3. Loss of *Acer1* Alters Skin Sphingolipids in Adult Mice

(A–H) Skin tissues isolated from P33 *Acer1*$^{+/+}$ and *Acer1*$^{-/-}$ mice were analyzed by LC-MS/MS (n = 4 individual mice) for (A) ceramides, (B) dihydroceramides, (C) phytoceramides, (D) α-hydroxy-ceramides, (E) monohexosyl-ceramides, (F) sphingomyelins, (G) sphingoid bases, and (H) their phosphates.

(I–K) qPCR results showing mRNA levels of other ceramidases (I), *Sgpp2* (J), and *Sphk1* and *SphK2* (K) and between P33 *Acer1*$^{+/+}$ and *Acer1*$^{-/-}$ mice. n = 3 individual mice.

The error bars indicate the SD.

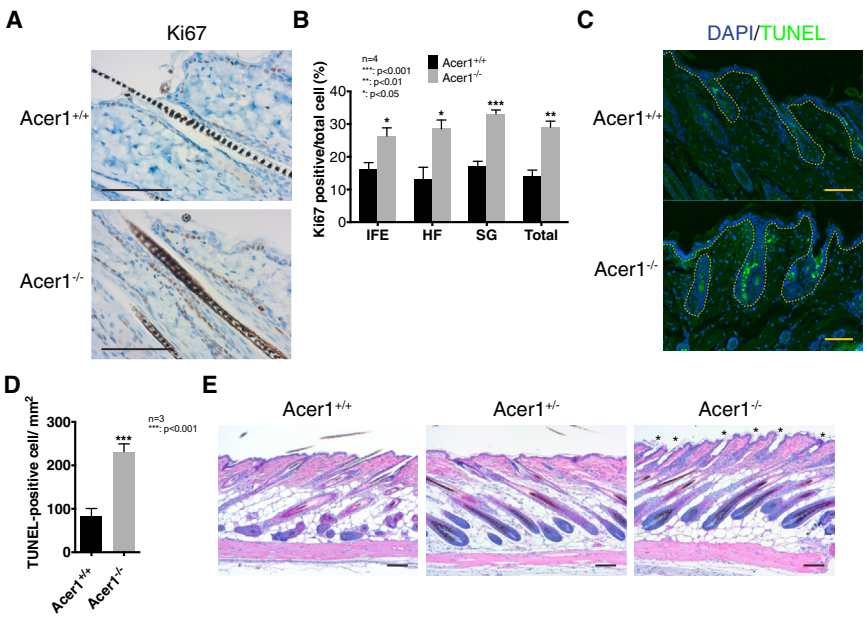

Figure 4. Loss of *Acer1* Increases the Proliferation and Apoptosis of Epidermal Keratinocytes while Dilating Pilary Canal

(A) IHC of skin tissue sections with anti-Ki-67 antibody.

(B) Quantification of Ki-67-positive cells in different compartments in the tissue sections from (A). n = 4 individual mice.

(C) Skin tissue sections from P64 *Acer1*$^{+/+}$ and *Acer1*$^{-/-}$ mice were stained with a TUNEL (green) assay kit and counterstained for nuclei with DAPI (blue). The yellowed dash lines separate the epidermis (upper) and dermis (lower) and outline the hair follicle.

(D) Quantification of apoptotic EKs from (C) by the value of TUNEL-positive cell versus area (mm^2). n = 3 individual mice.

(E) H&E staining of skins from P35 Acer$^{+/+}$, *Acer1*$^{+/-}$, and *Acer1*$^{-/-}$ mice.

Note abnormally dilated pilary canals marked with asterisks and lipid accumulation in pilary canals marked with stars in *Acer1*$^{-/-}$ mice. The error bars indicate the SD. Scale bar, 100 μm.

Taken together, these results suggest that loss of *Acer1* alters the morphology of the HF and disrupts the lipid secretory function of the SG.

Loss of *Acer1* Progressively Depletes the Population of Hair Follicle Stem Cells

The initiation of HF cycling involves HFSC reactivation in transition between telogen and anagen (Greco et al., 2009). Since we observed a delay in the telogen-to-anagen transition after depilation in *Acer1*$^{-/-}$ mice (Figures 1F and 1G), we postulated that *Acer1* loss might affect the homeostasis of HFSCs. To this end, we determined the HFSC population by measuring the number of label-retaining cells (LRC) or cells expressing CD34, a mouse quiescent HFSC marker. P3 newborns were injected with 5-ethynyl-2′-deoxyuridine (EdU) and chased for 4–6 weeks. EdU-retaining cells (EdU$^+$ LRC) were visualized and quantified using a Click-iT EdU immunofluorescence staining kit (Life Technologies). As shown in Figure 5A, we found that the number of LRCs was significantly reduced in *Acer1*$^{-/-}$ mice compared with *Acer1*$^{+/+}$ mice. Consistently, IHC showed that *Acer1*$^{-/-}$ mice had fewer CD34-positive cells in the bulge region of the HF compared with *Acer1*$^{+/+}$ mice (Figure 5B). Furthermore, IHC staining of skin tissues collected from mice at different ages showed an age-dependent reduction of CD34-postive cells (Figure 5C). To quantify the number of CD34-positive HFSCs more accurately, we performed flow cytometric analyses of HFSCs co-stained with antibodies against CD34 and integrin alpha 6 (α6). As shown in Figure 5D, the number of CD34/α6 double-positive cells were decreased in *Acer1*$^{-/-}$ mice in an age-dependent manner. Taken together, these results suggest that *Acer1* deficiency progressively reduces the HFSC population.

Loss of *Acer1* Reduces Hair Follicle Stem Cell Survival and Quiescence

To test if loss of *Acer1* affects the characteristics of HFSCs such as self-renewal and quiescence in a cell-autonomous mechanism, we performed colony formation assays with HFSCs isolated from *Acer1*$^{+/+}$ or *Acer1*$^{-/-}$ mice. HFSCs were isolated from P25 *Acer1*$^{+/+}$ and *Acer1*$^{-/-}$ mice in telogen, labeled with anti-CD34 and anti-a6 integrin antibodies, and sorted by fluorescence-activated cell sorting (FACS) as described in the Experimental Procedures. qPCR analyses confirmed that *Acer1* mRNA is expressed in *Acer1*$^{+/+}$ HFSCs but not in *Acer1*$^{-/-}$ HFSCs (Figure 5E). When the same number of viable *Acer1*$^{+/+}$ or *Acer1*$^{-/-}$ HFSCs were cultured over a monolayer of Swiss3T3 feeder cells, we found that *Acer1*$^{-/-}$ HFSCs formed fewer but larger colonies compared with *Acer1*$^{+/+}$ HFSCs (Figure 5F), indicating that loss of *Acer1* reduces HFSC survival or the colony formation ability (stemness) while enhancing their proliferation at least in part through a cell-autonomous mechanism.

To test whether loss of *Acer1* reduces the long-term maintenance of HFSCs, we cultured *Acer1*$^{+/+}$ or *Acer1*$^{-/-}$ HFSCs for three passages in a feeder-free 3C-Matrigel medium that maintains HFSC stemness much longer than the traditional 2D-feeder cell culture (Chacón Martínez et al., 2017).

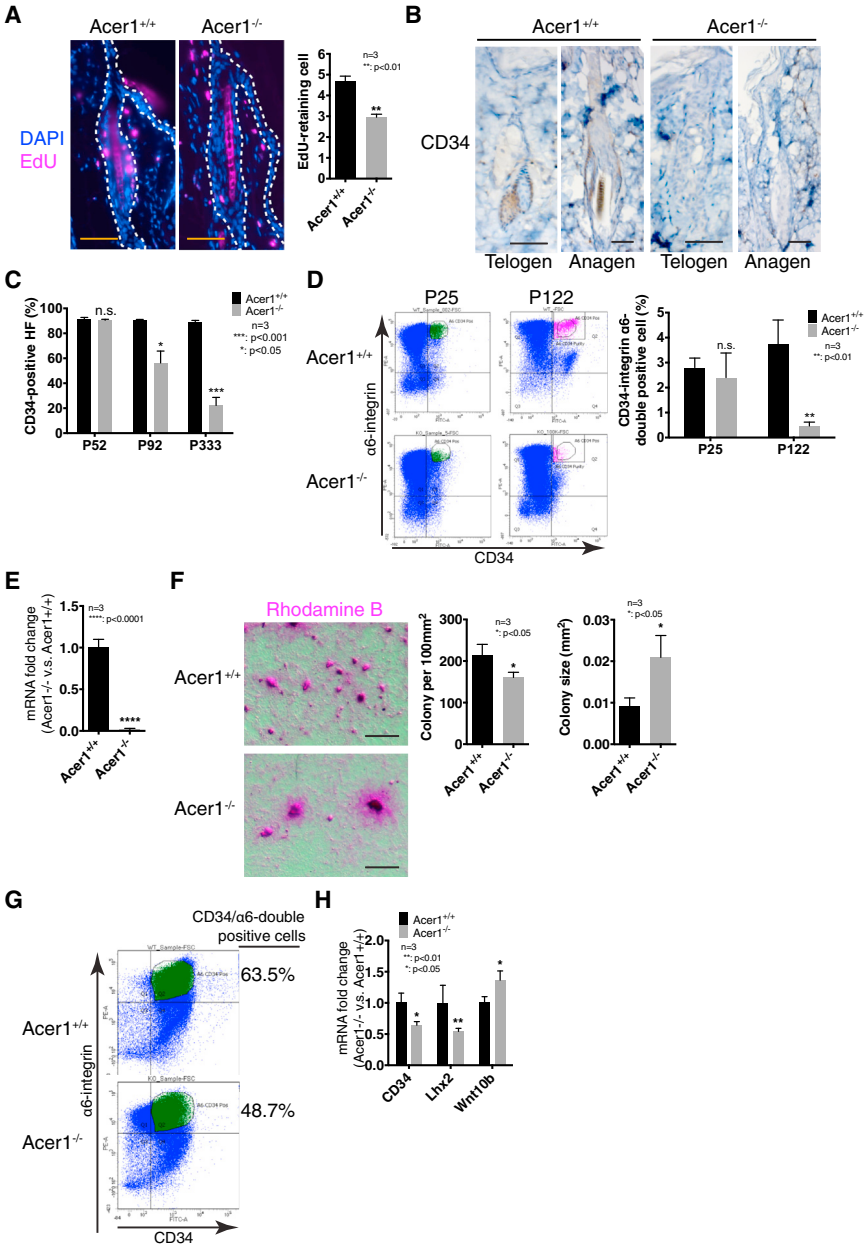

Figure 5. Loss of *Acer1* Progressively Depletes the Population of Quiescent HFSCs

(A) Left: LRCs in the HF from P50 *Acer1*$^{+/+}$ and *Acer1*$^{-/-}$ mice. The left panels, EdU; the middle panel, DAPI; and the right panel, EdU/DAPI merged. White dashed lines outline the HF and IFE. Right: Quantification of EdU-positive LRCs in the HF region. n = 3 individual mice. Scale bar, 50 μm.

(B) IHC of skin sections from P92 *Acer1*$^{+/+}$ and *Acer1*$^{+/-}$ mice with an antibody against the bulge stem cell marker CD34. Scale bar, 50 μm.

(C) Quantification of percentages of CD34-positive HF from different ages (P52, P92, and P333). n = 3 individual mice.

(D) Left: FACS sorting of FITC-CD34 (x axis) and PE-α6 (y axis) double-positive cells from P25 and P122 *Acer1*$^{+/+}$ and *Acer1*$^{-/-}$ mice. Right: Quantification of percentages of CD34/α6 double-positive cells. n = 3 individual mice.

(E) qPCR analysis of *Acer1* on primary cultured P25 *Acer1*$^{+/+}$ and *Acer1*$^{-/-}$ HFSCs.

(F) Left: Colony formation assays on primary *Acer1*$^{+/+}$ and *Acer1*$^{-/-}$ HFSCs cultured for 2 weeks. Scale bar, 1 mm. Right: Quantification of (F) by counting the number of colonies per 100 mm^2 and the average size of colonies (mm^2). n = 3 individual mice.

(G) FACS of CD34/α6 double-positive cells from HFSCs cultured in 3C media-Matrigel.

(H) qPCR analysis of HFSC quiescence markers (*CD34* and *Lhx2*) and HFSC activation signature gene *Wnt10b* on primary cultured *Acer1*$^{+/+}$ and *Acer1*$^{-/-}$ HFSCs. n = 3 individual mice.

The error bars indicate the SD.

This feeder-free culture condition allowed us to assess the percentage of cultured cells that retain the stem cell markers without contamination of feeder cells. As shown in Figure 5G, flow cytometry revealed that the CD34/integrin α6 double-positive cell population was much lower in the *Acer1*$^{-/-}$ HFSC culture than in the *Acer1*$^{+/+}$ HFSC culture, suggesting that loss of *Acer1* may reduce HFSC stemness in addition to HFSC survival.

As we observed that the colony size of *Acer1*$^{-/-}$ HFSCs is larger than that of *Acer1*$^{+/+}$ HFSCs (Figure 5F), we wanted to test whether loss of *Acer1* accelerates HSFC activation. To this end, we measured the mRNA levels of HFSC quiescent and activation signature genes in *Acer1*$^{+/+}$ and *Acer1*$^{-/-}$ HFSCs. With qPCR, we demonstrated that loss of *Acer1* reduced the mRNA levels of the quiescent markers *CD34* and *Lhx2* (Figure 5H) and elevated the mRNA levels of the activation signature gene *Wnt10b* (Figure 5H), suggesting that loss of *Acer1* reduces the ability of HFSCs to maintain quiescence.

DISCUSSION

Our group previously demonstrated that both the mouse ACER1 and its human counterpart are predominantly

expressed in the skin (Mao et al., 2003; Sun et al., 2008), but neither the skin compartment-specific expression of ACER1 nor its physiological role in skin homeostasis is clear. In this study, we generated a mouse strain in which the endogenous mouse *Acer1* gene was replaced with the bacterial *LacZ* gene so that we could study the tissue-specific expression of *Acer1* and its physiological role in the skin simultaneously. We confirmed that *Acer1* is predominantly expressed in the skin and further revealed that *Acer1* is highly expressed in different epidermal compartments (the IFE, HF, and SG) (Figures 2 and S3). We further demonstrated that ACER1 plays a key role in regulating the homeostasis of the epidermis, the HF in particular, by controlling the metabolism of ceramides and their metabolites, sphingoid bases, in major epidermal compartments.

Our group previously demonstrated that ACER1 catalyzes the hydrolysis of VLC ceramides *in vitro* (Sun et al., 2008). In this study, we demonstrated that knocking out *Acer1* decreased skin alkaline ceramidase activity on the VLC ceramide, $C_{24:1}$ ceramide, more significantly than that on the LC ceramide, $C_{18:1}$ ceramide, indicating that similar to human ACER1, mouse ACER1 may prefer VLC ceramides to LC ceramides as substrates. Loss of *Acer1* caused a marked increase in the levels of VLC and LC ceramides, phytoceramides, and α-hydroxyceramides in the skin, indicating that ACER1 catalyzes the hydrolysis of various ceramide species in the skin although its preferred substrates are VLC ceramides. Interestingly, loss of *Acer1* also markedly increased the levels of free sphingoid bases (SPH, DHS, and PHS) without affecting sphingoid base phosphates. This result was not expected because SPH, as a product of ACER1, should be increased in $Acer1^{-/-}$ mice. With the sphingolipid pathway-specific qPCR array that simultaneously analyzes mRNA levels of enzymes known to be involved in the metabolism of sphingolipids, we revealed that loss of *Acer1* upregulated the SPH-generating enzymes ACER2, ACER3, and SGPP2 (Figures 3I and 3J) while downregulating the enzymes SPHK1 and SPHK2, which convert SPH to its phosphate (Figure 3K). The changes in the expression of these enzymes may be responsible for the unexpected increase in the sphingoid base, but why and how these changes occur remain unclear. Taken together, these results suggest that ACER1 plays a key role, directly and by altering the expression of other enzymes, in regulating the homeostasis of sphingolipids in the skin.

Ceramides have been shown to act as bioactive lipids to regulate various biological processes (Hannun and Obeid, 2008). It was thought that all ceramides had the same role in cellular responses. However, emerging evidence indicates that different ceramide species may have different or even opposing roles in cellular processes. LC ceramides (C_{16} ceramide and C_{18} ceramide) have anti-proliferative effects such as cell-cycle arrest, senescence, and apoptosis (Saddoughi and Ogretmen, 2013), whereas VLC ceramides (C_{22}, C_{24}, and $C_{24:1}$ ceramide) have been shown to promote cell proliferation and cell survival (Grösch et al., 2012). Like ceramides, SPH, and other free sphingoid bases have been shown to act as signaling molecules to mediate cell growth arrest, autophagy, and apoptosis (Cuvillier, 2002; Cuvillier et al., 2001; Hu et al., 2005; Kim et al., 2004; Nava et al., 2000; Vogler et al., 2003; Xu et al., 2006, 2016; Yi et al., 2016). These results indicate that as a key enzyme in regulating ceramides and sphingoid bases in the epidermis, loss of *Acer1* is expected to trigger profound effects on the biology of the epidermis.

Indeed, in this study, we demonstrated that loss of *Acer1* exerts effects on cell proliferation, differentiation, and survival in epidermal compartments. We demonstrated that loss of *Acer1* inhibited the expression of various keratinocyte differentiation markers, such as cytokeratin 1 (K1) and cytokeratin 10 (K10), suggesting a role for ACER1 in keratinocyte differentiation. Consistently, in our previous study, we found that knocking down human ACER1 also inhibited Ca^{2+}-induced differentiation of epidermal keratinocytes in culture (Sun et al., 2008). As *Acer1* knockout and *Acer1* knockdown have a similar effect on ceramides but an opposing effect on SPH, we speculated that ACER1 mediates keratinocyte differentiation likely through ceramides rather than SPH and other sphingoid bases. Although loss of *Acer1* significantly decreases K1 and K10, $Acer1^{-/-}$ mice appear to have a normal structure of the IFE as $Acer1^{+/+}$ mice, suggesting that loss of *Acer1* may have a mild effect on epidermal differentiation. In this study, we also found that loss of *Acer1* enhanced the proliferation of cells in different compartments of the epidermis. The proliferative effect could be caused by a marked increase in the levels of various VLC ceramides, phytoceramides, and/or α-hydroxyceramides. Unexpectedly, loss of *Acer1* also increased apoptosis of cells in different compartments of the epidermis (Figures 4C and 4D), although our previous study found that knocking down the human *Acer1* did not lead to apoptosis of epidermal keratinocytes in culture. As loss of *Acer1* accumulated both LC ceramides and free sphingoid bases in the epidermis, whereas *Acer1* knockdown only accumulated VLC ceramides, we postulated that loss of *Acer1* led to apoptosis of cells in the epidermis likely due to accumulation of LC ceramides and/or free sphingoid bases. In agreement with this notion, Uchida et al. (2010) demonstrated that blocking the acid ceramidase (ASAH1) and neutral ceramidase (ASAH2) enhances both the generation of LC ceramides and the apoptosis of epidermal keratinocytes in response to UV radiation (UVR), and Tolleson et al. (1999) found that treatment with the ceramide synthase inhibitor fumonisin B1 (FB1)

accumulated free DHS in epidermal keratinocytes and led to the death of these cells.

Emerging evidence suggests that the metabolism of ceramides in the epidermis plays a key role in hair growth and maintenance (Ebel et al., 2014; Peters et al., 2015). Loss of *Cers4*, which is responsible for the synthesis of LC ceramides ($C_{18\text{-}20}$ ceramides), results in age-related hair loss in mice. Interestingly, in this study, we demonstrated that loss of *Acer1*, responsible for the hydrolysis of epidermal ceramides, also led to progressive hair loss in mice. Although Cers4 catalyzes a different reaction from ACER1, loss of *Cers4* causes similar effects on sphingolipids as loss of *Acer1*, accumulating various ceramide species ($C_{16:0}$-, $C_{24:0}$-Cer, $C_{22:0}$-, and $C_{24:0}$-hydroxy-ceramide) while reducing the levels of its substrates $C_{18\text{-}20}$ ceramides in the skin (Peters et al., 2015). The similar changes in these ceramide species may explain why mice deficient in *Acer1* and *Cers4* have a similar hair loss phenotype and suggest that accumulated ceramides are indeed responsible for hair loss in mice.

We demonstrated that loss of *Acer1* caused the hypertrophy of SG and accumulation of lipids in the HF infundibulum while decreasing lipids on the surface of the epidermis. Lipid accumulation in the HF infundibulum may cause abnormality in the structure of the HF. It has been proposed that age-related accumulation of lipids in the HF infundibulum impairs the maintenance of the hair shaft and thereby leads to progressive alopecia (Ebel et al., 2014). These results suggest that loss of *Acer1* induces progressive hair loss in part due to impairments in both the structure and function of the SG. We found that loss of *Acer1* also progressively decreased the HFSC population in mice, indicating that ACER1 is critical for the homeostasis of the HFSC. Taken together, these results suggest that loss of *Acer1* causes alopecia in mice by breaching both the lipid secretory function of the SG and the homeostasis of HFSCs.

Our results indicate that loss of *Acer1* leads to HFSC depletion probably due to a decrease in stem cell survival and/or quiescence. We found that loss of *Acer1* altered HF cycling by increasing the length of the resetting phase while shortening the following phases (Figures 1F and 1G), indicating that loss of *Acer1* accelerates hair cycling. Similar to loss of *Acer1*, Ebel et al. (2014) showed that loss of *Cers4* also accelerates HF cycling. These results suggest that increased ceramides in the epidermis may accelerate HF cycling. There are many other mouse genes whose inactivation accelerates HF cycling and HFSC depletion, resulting in hair loss (Nakajima et al., 2013; Oda et al., 2012). These results suggest that loss of *Acer1* causes HFSC depletion in part by accelerating hair cycling. Accelerated hair cycling in $Acer^{-/-}$ mice may be caused by loss of quiescence or increased activation of HFSCs. In line with this notion, we demonstrated that when cultured with feeder cells *in vitro*, $Acer1^{-/-}$ HFSCs formed large colonies and lost HSFC markers more quickly than $Acer1^{+/+}$ HFSCs (Figure 5E). Cell counting showed that $Acer1^{-/-}$ HFSCs form larger colonies because of an increase in cell proliferation (Figure S5A). These results suggest that loss of *Acer1* indeed reduces the ability of HFSCs to main quiescence. In addition to the difference in colony size, we also found that fewer colonies were formed from $Acer1^{-/-}$ HFSCs than from $Acer1^{+/+}$ HFSCs when the same number of these cells was plated on a feeder layer (Figure 5E), suggesting that loss of *Acer1* may reduce HFSC survival as well. In addition to the cell-autonomous effects on HFSCs, *Acer1* deficiency may deplete HFSCs also through a non-cell-autonomous mechanism because *Acer1* is highly expressed in different cell types in the hair follicle. Taken together, these results suggest that loss of *Acer1* impairs the homeostasis of HFSCs by enhancing their proliferation and inhibiting their survival and quiescence through both cell and non-cell-autonomous mechanisms.

Loss of *Acer1* reduces HFSC quiescence or increases HFSC activation probably by regulating the Lhx2 and/or Wnt signaling pathway. With qPCR analyses, we found that loss of *Acer1* reduced the mRNA levels of the transcription factor Lhx2 (LIM homeobox 2), which has been implicated in the maintenance of quiescence of HFSCs (Rhee et al., 2006). Similar to loss of *Acer1*, loss of *Lhx2* significantly reduces CD34 (Folgueras et al., 2013) and the LRC population, increases cell proliferation in the epidermis (Rhee et al., 2006), disrupts HF architecture, and causes baldness (Folgueras et al., 2013). Interestingly, loss of *Acer1* did not reduce the expression of the *Sox9*, *Nfatc1*, and *Lgr5* in HFSCs (Figure S6B), although these genes are known downstream targets of *Lhx2* (Kim and Kim, 2014; Kim et al., 2014; Mardaryev et al., 2011), suggesting that loss of *Acer1* reduces HFSC quiescence through an unknown target(s) of Lhx2. In contrast to Lhx2, loss of *Acer1* increased the mRNA levels of Wnt10b in HFSCs (Figure 5G). *Wnt10b* serves a signature gene of transit-amplifying cells and plays an important role in stem cell quiescence (Lim et al., 2016) and anagen activation (Li et al., 2013). These results suggest that loss of *Acer1* may reduce the quiescence of HFSCs in part by inhibiting Lhx2 and/or activating the Wnt pathway.

While we were preparing this manuscript, Liakath Ali et al. (2016) reported similar findings to ours regarding the hair loss phenotype in a different knockout strain. They reported several SG abnormalities in $Acer1^{-/-}$ mice, such as a different adipocyte arrangement, lipid droplet structure, and nuclear shape (Liakath Ali et al., 2016), thus explaining why loss of *Acer1* impairs the secretion of neutral lipids to the skin surface via the HF infundibulum. In addition, Liakath Ali et al. (2016) showed increased

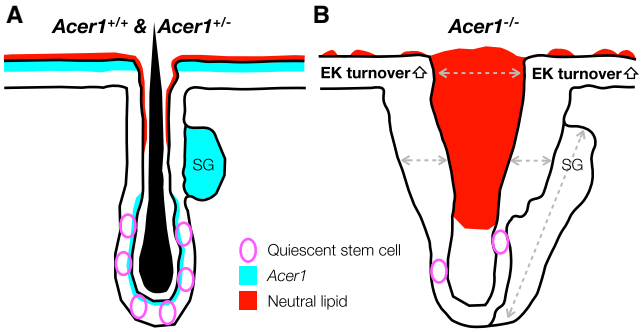

Figure 6. Model Describing the Role of ACER1 in the Homeostasis of the Different Compartments of the Epidermis

This figure depicts the structural and functional differences between the epidermis from (A) *Acer1*$^{+/+}$/*Acer1*$^{+/-}$ and (B) *Acer1*$^{-/-}$ mice. *Acer1* is expressed in the IFE, SG, and bulge regions in *Acer1*$^{+/+}$/*Acer1*$^{+/-}$ mice (A), and upon loss of *Acer1*, both ceramides (Cer) and sphingoid bases (SPH) are accumulated in these epidermal compartments in *Acer1*$^{-/-}$ mice. Accumulated sphingolipids lead to the hypertrophy of IFE and SG, widening of the pilary canal (gray dashed double-headed arrows), the accumulation of lipids (red), and the depletion of HFSCs. Purple circles represent quiescent stem cells and cyan color represents *Acer1* expression.

trans-epidermal water loss and hyper-metabolism in *Acer1*$^{-/-}$ mice, suggesting alterations in energy balance and thermal insulation. This may explain why loss of *Acer1* causes body weight loss in middle-aged or older mice, another important phenotypic change observed by both studies. However, there is one major discrepancy between our studies and theirs. We demonstrated that loss of *Acer1* increased the levels of free sphingoid bases without affecting the levels of sphingoid base phosphates or complex sphingolipids (monohexosylceramides and sphingomyelins) in the skin, while Liakath Ali et al. (2016) showed that there were significant decreases in the levels of sphingoid bases and their phosphates and increases in the levels of complex sphingolipids in the skins of *Acer1*$^{-/-}$ mice compared with *Acer1*$^{+/+}$ mice (Figure 3). These differences do not appear to be caused by the use of different mouse strains because we showed that loss of *Acer1* caused the same changes in the sphingolipid profile in mice with an FVB background (our unpublished data). These differences could be due to the ways in which skin tissues were prepared for lipid analyses. We analyzed sphingolipids in the whole skin, which encompasses different epidermal compartments where *Acer1* is expressed, whereas Liakath Ali et al. (2016) did so only in the stratum corneum where no *Acer1* is expressed. In addition, we but not Liakath Ali et al. (2016) revealed the role of ACER1 in regulating the homeostasis of HFSCs and made significant progress in understanding the mechanism by which ACER1 maintains the homeostasis of HFSCs.

In conclusion, we demonstrated that the skin-specific ceramidase ACER1 regulates the metabolism of ceramides and sphingoid bases in the skin as well as homeostasis of the SG and HF so loss of *Acer1* results in progressive HFSC depletion and alopecia (Figure 6). Along with other previous studies, our study suggests that tight regulation of the metabolism of ceramides and free sphingoid bases is critical for the homeostasis of HFSCs, the epidermis, and its appendages.

EXPERIMENTAL PROCEDURES

Animals

All mice used in this study were housed under conventional laboratory conditions at a constant room temperature (RT, 22°C), humidity level (55%), 12-hr light/12-hr dark cycle, and food (W.F. Fisher & Son) and water available *ad libitum*. The generation of mice heterozygous for the *Acer1* null allele, *Acer1*$^{+/-}$ mice, was approved by the Institutional Animal Care and Use Committee (IACUC) of the University of California at Davis (UC Davis). All other animal studies were performed following procedures approved by the IACUC at Stony Brook University (Stony Brook, NY).

Acer1 Null C57BL/6J Mice

A gene-trap embryonic stem cell clone (18475A-H9) in which one copy of the whole open-reading frame (ORF) of the mouse *Acer1* gene was replaced by a gene cassette containing the reporter gene *LacZ* and the neomycin resistant gene (*Neo*) (Figure 1A) was created by Regeneron Pharmaceuticals using VelociGene technology as described (Valenzuela et al., 2003). This embryonic stem cell clone was made into live mice by the Repository Knockout Mouse Project (KOMP) at the University of California at Davis. Briefly, embryonic stem cells expanded from the 18475A-H9 clone were injected into C57BL/6J blastocysts, which were transplanted into the uteri of pseudopregnant C57BL/6J mice. The resulting chimeric mice were crossed to WT C57BL/6J mice to generate offspring heterozygous for the *Acer1* null allele, *Acer1*$^{+/-}$ mice, which were inbred to generate *Acer1* null (*Acer1*$^{-/-}$) mice and their *Acer1*$^{+/+}$ and *Acer1*$^{+/-}$ littermates.

Statistics

Statistical analyses were performed using an unpaired two-tailed Student's t test. The p values for significance are stated in the figures (*$p > 0.05$; **$p > 0.01$; ***$p > 0.001$). The error bars indicate the SD.

qPCR

Skin RNAs were extracted, reverse transcribed into cDNAs (Wang et al., 2015), and subjected to qPCR analyses using the primer pairs listed in Table S1. qPCR was performed and analyzed with the ABI Prism 7000 system (Applied Biosystems) using the ΔΔCt method with *β-Actin* as an internal control as described (Mao et al., 2003).

Alkaline Ceramidase Activity Assay

Skin tissues were harvested from P0 newborn mice, and alkaline ceramidase activity was measured using D-*e*-$C_{24:1}$ ceramide or

D-*e*-$C_{18:1}$ ceramide as a substrate according to the protocol that we developed previously (Wang et al., 2015).

HF Cycle Monitoring

To determine the length of the first anagen of the HF cycle, P21 mice were shaved on the back and the shaved areas were photographed daily to record color changes with time. To monitor HF cycling after the first anagen, the HF cycle was synchronized in telogen. Mice were depilated by applying bikini wax onto their backs, and the colors of the depilated areas were monitored daily as described above. The stage of the HF cycle was determined by the skin color as described (Muller-Rover et al., 2001).

In Situ β-Galactosidase Assay

Freshly obtained tissues were embedded in optimal cutting temperature compound (Tissue Tek). Cryosections were done at 5 μm on a cryostat set at −25°C. For *in situ* β-galactosidase activity assays, sections were fixed for 10 min at 4°C in 0.5% glutaraldehyde/PBS. Samples were then washed with PBS three times for 5 min each and stained for 6–24 hr at 37°C with X-gal working solution with 1 mg/mL X-gal in PBS, 5 mM $K_3Fe(CN)_6$, and 5 mM $K_4Fe(CN)_6$, and counterstained with nuclear fast red (Vector Labs) or eosin (Sigma) (Folgueras et al., 2013).

LC-MS/MS Sphingolipid Analysis

Skin tissues collected from *Acer1*$^{+/+}$ or *Acer1*$^{-/-}$ mice at different ages and skin sphingolipids were analyzed by liquid chromatography-tandem mass spectrometry (LC-MS/MS) as described (Bielawski et al., 2006) in the Lipidomics Core Facility at Stony Brook University.

Histology

Mouse dorsal skin tissues were harvested, fixed in 10% formalin, embedded in paraffin, and sectioned at 5 μm. Deparaffined and rehydrated sections were stained with H&E.

Immunohistochemistry Staining

IHC staining was done as described in our previous study (Wang et al., 2015). Briefly, skin sections were deparaffined and rehydrated, antigens were retrieved, and endogenous peroxidase activity was quenched. Sections were stained by Thermo Fisher Histostain-Plus Kit (Thermo Fisher), incubated with 1.1 mM DAB (3,3′-diaminobenzidine tetrahydrochloride hydrate, D5637, Sigma), and counterstained with hematoxylin (Sigma). The stained tissue sections were imaged under a Zeiss fluorescent microscope.

Immunofluorescence Staining

Skin tissue cryosections were fixed with 4% paraformaldehyde for 10 min, permeabilized with 0.1% Triton X-100 in PBS for 15 min, and washed with PBS three times, 5 min each, at RT, blocked with 1% goat serum at RT for 30 min, incubated with a primary antibody at 4°C overnight, followed by a corresponding fluorophore-conjugated secondary antibody (1:400; Jackson ImmunoResearch) for 45 min, and counterstained with 1 μg/mL of DAPI/PBS for 10 min before being imaged under the Zeiss fluorescent microscope.

Analysis of Skin Label-Retaining Cells

For newborn LRC analysis, *Acer1*$^{+/+}$, *Acer1*$^{+/-}$, and *Acer1*$^{-/-}$ newborns (P0) were injected with EdU (100 mg/g body weight) daily for 4 consecutive days. At 1 month of age (P31), the mice were euthanized, the dorsal skins were isolated, paraffin-embedded, sectioned, and the resulting sections were subjected to EdU staining using a Click-iT EdU Alexa Fluor 562 Imaging Kit (Life Technologies).

Fluorescence-Activated Cell Sorting

Sorting was done as described (Nowak and Fuchs, 2009). Briefly, epidermis was separated from the whole skin by 0.25% EDTA-free trypsin treatment at 4°C overnight. Single cells were selected by passing through a 70 μm cell strainer followed by a 40 μm cell strainer. Cells were incubated with FITC-CD34 and PE-integrin α6 antibodies (Table S3) at RT for 30 min. CD34/α6 double-positive cells were sorted out by FACS on a BD FACSAria III system (BD Biosciences), compared with negative controls without adding antibodies, and collected to E media (Nowak and Fuchs, 2009) and seeded onto the mitomycin C-treated Swiss 3T3 feeder cells on 12-well or 24-well culture plates with 0.3 mM $CaCl_2$.

Colony Formation Assay

CD34/α6 double-positive cells were cultured with feeder cells on a 12-well culture plate for 14–21 days until colonies became visible. Cell cultures were washed with PBS before being fixed with 4% paraformadehyde at RT for 10 min. The fixed cell cultures were washed with PBS and stained with 2% Rhodamine B (Sigma)/d_2H_2O at RT.

Feeder-free Culture of HFSC

HFSC were cultured in feeder-free 3C media in Matrigel as described (Chacón Martínez et al., 2017). Briefly, 3C media is modified from E media (Nowak and Fuchs, 2009) by adding 10 ng/mL EGF, 5 ng/mL transferrin, 5 μM Y27632, 20 ng/mL mouse recombinant VEGF-A, 20 ng/mL human recombinant FGF-2 (Sigma), and 0.3 mM $CaCl_2$. 2.5×10^4 cells were suspended in 40 μL of an ice-cold 1:1 mixture of 3C media and growth-factor-reduced Matrigel (Corning) dispensed as a droplet in a 24-well culture plate.

Terminal Deoxynucleotidyl Transferase dUTP Nick End Labeling Assay

Apoptotic cells were assessed using a DeadEnd Fluorometric TUNEL System (Promega). Briefly, deparaffinized skin sections were permeabilized by immersing in 20 μg/mL of Proteinase K at RT for 10 min, and equilibrated in an equilibrium buffer at RT for 10 min before fragmented DNAs were labeled with a TdT reaction mix at 37°C for 1 hr and then stopped by immersing the tissue sections in 2× SCC buffer. The tissue sections were counterstained with 1 μg/mL of DAPI/PBS for 10 min before being imaged under a Zeiss fluorescent microscope.

Antibodies

Primary antibodies used for IHC, IF, FACS, and western blotting are listed in Table S3.

SUPPLEMENTAL INFORMATION

Supplemental Information includes Supplemental Experimental Procedures, six figures, and three tables and can be found with this article online at https://doi.org/10.1016/j.stemcr.2017.09.015.

AUTHOR CONTRIBUTIONS

C.-L.L. and C.M. conceived and designed experiments; C.-L.L. and R.X. generated knockout mice; C.-L.L., R.X., J.K.Y., and F.L. performed experiments; J. Cao, L.H., and B.R. contributed to reagents and equipment; J. Chen, E.C.J., J.B.S., X.Z., A.J.S., L.M.O., and Y.A.H. contributed to interpretation of data and manuscript editing. C.-L.L. and C.M. wrote the manuscript.

ACKNOWLEDGMENTS

This work was supported, in whole or in part, by NIH grants P01 CA097132 (to Y.A.H., L.M.O., and C.M.), R01CA104834 (to C.M.), and R01CA163825 (to C.M.) and a Veterans Affairs Merit Award (to L.M.O.).

Received: September 8, 2016
Revised: September 20, 2017
Accepted: September 21, 2017
Published: October 19, 2017

REFERENCES

Alonso, L., and Fuchs, E. (2006). The hair cycle. J. Cell Sci *119*, 391–393.

Bielawski, J., Szulc, Z.M., Hannun, Y.A., and Bielawska, A. (2006). Simultaneous quantitative analysis of bioactive sphingolipids by high-performance liquid chromatography-tandem mass spectrometry. Methods *39*, 82–91.

Chacón Martínez, C.A., Klose, M., Niemann, C., Glauche, I., and Wickström, S.A. (2017). Hair follicle stem cell cultures reveal self-organizing plasticity of stem cells and their progeny. EMBO J. *36*, 151–164.

Courtois, M., Loussouarn, G., and seau, C. (1994). Hair cycle and alopecia. Skin Pharmacol. *7*, 84–89.

Cuvillier, O. (2002). Sphingosine in apoptosis signaling. Biochim. Biophys. Acta *1585*, 153–162.

Cuvillier, O., Nava, V.E., Murthy, S.K., Edsall, L.C., Levade, T., Milstien, S., and Spiegel, S. (2001). Sphingosine generation, cytochrome c release, and activation of caspase-7 in doxorubicin-induced apoptosis of MCF7 breast adenocarcinoma cells. Cell Death Differ. *8*, 162–171.

Ebel, P., Imgrund, S., Vom Dorp, K., Hofmann, K., Maier, H., Drake, H., Degen, J., Dormann, P., Eckhardt, M., Franz, T., et al. (2014). Ceramide synthase 4 deficiency in mice causes lipid alterations in sebum and results in alopecia. Biochem. J. *461*, 147–158.

Folgueras, A.R., Guo, X., Pasolli, H.A., Stokes, N., Polak, L., Zheng, D., and Fuchs, E. (2013). Architectural niche organization by LHX2 is linked to hair follicle stem cell function. Cell Stem Cell *13*, 314–327.

Fuchs, E. (2007). Scratching the surface of skin development. Nature *445*, 834–842.

Greco, V., Chen, T., Rendl, M., Schober, M., Pasolli, H.A., Stokes, N., dela Cruz-Racelis, J., and Fuchs, E. (2009). A two-step mechanism for stem cell activation during hair regeneration. Stem Cell *4*, 155–169.

Grösch, S., Schiffmann, S., and Geisslinger, G. (2012). Chain length-specific properties of ceramides. Prog. Lipid Res. *51*, 50–62.

Hannun, Y.A., and Obeid, L.M. (2008). Principles of bioactive lipid signalling: lessons from sphingolipids. Nat. Rev. Mol. Cell Biol. *9*, 139–150.

Houben, E., Holleran, W.M., Yaginuma, T., Mao, C., Obeid, L.M., Rogiers, V., Takagi, Y., Elias, P.M., and Uchida, Y. (2006). Differentiation-associated expression of ceramidase isoforms in cultured keratinocytes and epidermis. J. Lipid Res. *47*, 1063–1070.

Hsu, Y.C., Li, L., and Fuchs, E. (2014). Emerging interactions between skin stem cells and their niches. Nat. Med. *20*, 847–856.

Hu, W., Xu, R., Sun, W., Szulc, Z.M., Bielawski, J., Obeid, L.M., and Mao, C. (2010). Alkaline ceramidase 3 (ACER3) hydrolyzes unsaturated long-chain ceramides, and its down-regulation inhibits both cell proliferation and apoptosis. J. Biol. Chem. *285*, 7964–7976.

Hu, W., Xu, R., Zhang, G., Jin, J., Szulc, Z.M., Bielawski, J., Hannun, Y.A., Obeid, L.M., and Mao, C. (2005). Golgi fragmentation is associated with ceramide-induced cellular effects. Mol. Biol. Cell *16*, 1555–1567.

Jennemann, R., Rabionet, M., Gorgas, K., Epstein, S., Dalpke, A., Rothermel, U., Bayerle, A., van der Hoeven, F., Imgrund, S., Kirsch, J., et al. (2012). Loss of ceramide synthase 3 causes lethal skin barrier disruption. Hum. Mol. Genet. *21*, 586–608.

Kim, D.S., Kim, S.Y., Kleuser, B., Schafer-Korting, M., Kim, K.H., and Park, K.C. (2004). Sphingosine-1-phosphate inhibits human keratinocyte proliferation via Akt/protein kinase B inactivation. Cell. Signal. *16*, 89–95.

Kim, J.H., and Kim, N. (2014). Regulation of NFATc1 in osteoclast differentiation. J. Bone Metab. *21*, 233–241.

Kim, J.H., Youn, B.U., Kim, K., Moon, J.B., Lee, J., Nam, K.-I.I., Park, Y.-W., O'Leary, D.D.M., Kim, K.K., and Kim, N. (2014). Lhx2 regulates bone remodeling in mice by modulating RANKL signaling in osteoclasts. Cell Death Differ. *21*, 1613–1621.

Levy, M., and Futerman, A.H. (2010). Mammalian ceramide synthases. IUBMB Life *62*, 347–356.

Li, Y.-H., Zhang, K., Yang, K., Ye, J.-X., Xing, Y.-Z., Guo, H.-Y., Deng, F., Lian, X.-H., and Yang, T. (2013). Adenovirus-Mediated Wnt10b overexpression induces hair follicle regeneration. J. Invest. Dermatol. *133*, 42–48.

Liakath Ali, K., Vancollie, V.E., Lelliott, C.J., Speak, A.O., Lafont, D., Protheroe, H.J., Ingvorsen, C., Galli, A., Green, A., Gleeson, D., et al. (2016). Alkaline ceramidase 1 is essential for mammalian skin homeostasis and regulating whole body energy expenditure. J. Pathol. *239*, 374–383.

Lim, X., Tan, S.H., Yu, K.L., Lim, S.B.H., and Nusse, R. (2016). Axin2 marks quiescent hair follicle bulge stem cells that are maintained by autocrine Wnt/β-catenin signaling. Proc. Natl. Acad. Sci. USA *113*, E1498–E1505.

Mao, C., and Obeid, L.M. (2008). Ceramidases: regulators of cellular responses mediated by ceramide, sphingosine, and sphingosine-1-phosphate. Biochim. Biophys. Acta *1781*, 424–434.

Mao, C., Xu, R., Szulc, Z.M., Bielawski, J., Becker, K.P., Bielawska, A., Galadari, S.H., Hu, W., and Obeid, L.M. (2003). Cloning and characterization of a mouse endoplasmic reticulum alkaline ceramidase: an enzyme that preferentially regulates metabolism of very long chain ceramides. J. Biol. Chem. *278*, 31184–31191.

Mardaryev, A.N., Meier, N., Poterlowicz, K., Sharov, A.A., Sharova, T.Y., Ahmed, M.I., Rapisarda, V., Lewis, C., Fessing, M.Y., Ruenger, T.M., et al. (2011). Lhx2 differentially regulates Sox9, Tcf4 and Lgr5 in hair follicle stem cells to promote epidermal regeneration after injury. Development *138*, 4843–4852.

Muller-Rover, S., Handjiski, B., van der Veen, C., Eichmuller, S., Foitzik, K., McKay, I.A., Stenn, K.S., and Paus, R. (2001). A comprehensive guide for the accurate classification of murine hair follicles in distinct hair cycle stages. J. Invest. Dermatol. *117*, 3–15.

Nakajima, T., Inui, S., Fushimi, T., Noguchi, F., Kitagawa, Y., Reddy, J.K., and Itami, S. (2013). Roles of MED1 in quiescence of hair follicle stem cells and maintenance of normal hair cycling. J. Invest. Dermatol. *133*, 354–360.

Nakamura, M., Schneider, M.R., Schmidt-Ullrich, R., and Paus, R. (2013). Mutant laboratory mice with abnormalities in hair follicle morphogenesis, cycling, and/or structure: an update. J. Dermatol. Sci. *69*, 6–29.

Nava, V.E., Cuvillier, O., Edsall, L.C., Kimura, K., Milstien, S., Gelmann, E.P., and Spiegel, S. (2000). Sphingosine enhances apoptosis of radiation-resistant prostate cancer cells. Cancer Res. *60*, 4468–4474.

Nowak, J.A., and Fuchs, E. (2009). Isolation and culture of epithelial stem cells. Methods Mol. Biol. *482*, 215–232.

Oda, Y., Hu, L., Bul, V., Elalieh, H., Reddy, J.K., and Bikle, D.D. (2012). Coactivator MED1 ablation in keratinocytes results in hair-cycling defects and epidermal alterations. J. Invest. Dermatol. *132*, 1075–1083.

Pappas, A. (2009). Epidermal surface lipids. Dermatoendocrinol *1*, 72–76.

Peters, F., Vorhagen, S., Brodesser, S., Jakobshagen, K., Bruning, J.C., Niessen, C.M., and Kronke, M. (2015). Ceramide synthase 4 regulates stem cell homeostasis and hair follicle cycling. J. Invest. Dermatol. *135*, 1501–1509.

Rhee, H., Polak, L., and Fuchs, E. (2006). Lhx2 maintains stem cell character in hair follicles. Science *312*, 1946–1949.

Saddoughi, S.A., and Ogretmen, B. (2013). Diverse functions of ceramide in cancer cell death and proliferation. Adv. Cancer Res. *117*, 37–58.

Sotiropoulou, P.A., and Blanpain, C. (2012). Development and homeostasis of the skin epidermis. Cold Spring Harb. Perspect. Biol. *4*, a008383.

Stenn, K.S., and Paus, R. (2001). Controls of hair follicle cycling. Physiol. Rev. *81*, 449–494.

Sun, W., Xu, R., Hu, W., Jin, J., Crellin, H.A., Bielawski, J., Szulc, Z.M., Thiers, B.H., Obeid, L.M., and Mao, C. (2008). Upregulation of the human alkaline ceramidase 1 and acid ceramidase mediates calcium-induced differentiation of epidermal keratinocytes. J. Invest. Dermatol. *128*, 389–397.

Tolleson, W.H., Couch, L.H., Melchior, W.B., Jr., Jenkins, G.R., Muskhelishvili, M., Muskhelishvili, L., McGarrity, L.J., Domon, O., Morris, S.M., and Howard, P.C. (1999). Fumonisin B1 induces apoptosis in cultured human keratinocytes through sphinganine accumulation and ceramide depletion. Int. J. Oncol. *14*, 833–843.

Uchida, Y., Houben, E., Park, K., Douangpanya, S., Lee, Y.-M., Wu, B.X., Hannun, Y.A., Radin, N.S., Elias, P.M., and Holleran, W.M. (2010). Hydrolytic pathway protects against ceramide-induced apoptosis in keratinocytes exposed to UVB. J. Invest. Dermatol. *130*, 2472–2480.

Valenzuela, D.M., Murphy, A.J., Frendewey, D., Gale, N.W., Economides, A.N., Auerbach, W., Poueymirou, W.T., Adams, N.C., Rojas, J., Yasenchak, J., et al. (2003). High-throughput engineering of the mouse genome coupled with high-resolution expression analysis. Nat. Biotechnol. *21*, 652–659.

Vogler, R., Sauer, B., Kim, D.S., Schafer-Korting, M., and Kleuser, B. (2003). Sphingosine-1-phosphate and its potentially paradoxical effects on critical parameters of cutaneous wound healing. J. Invest. Dermatol. *120*, 693–700.

Wang, K., Xu, R., Schrandt, J., Shah, P., Gong, Y.Z., Preston, C., Wang, L., Yi, J.K., Lin, C.-L., Sun, W., et al. (2015). Alkaline ceramidase 3 deficiency results in Purkinje cell degeneration and cerebellar ataxia due to dyshomeostasis of sphingolipids in the brain. PLoS Genet. *11*, e1005591.

Xu, R., Jin, J., Hu, W., Sun, W., Bielawski, J., Szulc, Z., Taha, T., Obeid, L.M., and Mao, C. (2006). Golgi alkaline ceramidase regulates cell proliferation and survival by controlling levels of sphingosine and S1P. FASEB J. *20*, 1813–1825.

Xu, R., Wang, K., Mileva, I., Hannun, Y.A., Obeid, L.M., and Mao, C. (2016). Alkaline ceramidase 2 and its bioactive product sphingosine are novel regulators of the DNA damage response. Oncotarget *7*, 18440–18457.

Yi, J.K., Xu, R., Jeong, E., Mileva, I., Truman, J.-P., Lin, C.-L., Wang, K., Snider, J., Wen, S., Obeid, L.M., et al. (2016). Aging-related elevation of sphingoid bases shortens yeast chronological life span by compromising mitochondrial function. Oncotarget *7*, 21124–21144.